International Journal of Nanomedicine

Dovepress
Taylor & Francis Group

Open Access Full Text Article

ORIGINAL RESEARCH

Enhanced Cancer Immunotherapy by Bacterial Cytoplasmic Membranes Coated Nanovaccines for Co-Delivery of Ovalbumin Antigen and Immune Adjuvants to Dendritic Cells in Lymph Nodes

Peiqi Zhao[1], Yali Fan[2], Ziyou Wang[2], Heyun Tang[2], Yu Tian[3], Yingying Zhang[2]

[1]Department of Lymphoma, Tianjin's Clinical Research Center for Cancer, Key Laboratory of Cancer Prevention and Therapy, National Clinical Research Center for Cancer, Tianjin Medical University Cancer Institute and Hospital, Tianjin Medical University, Tianjin, 300060, People's Republic of China; [2]School of Medical Imaging, Xuzhou Medical University, Xuzhou, 221004, People's Republic of China; [3]School of Chemical Biology and Biotechnology, Peking University Shenzhen Graduate School, Shenzhen, People's Republic of China

Correspondence: Yu Tian; Yingying Zhang, Email tianyu@stu.pku.edu.cn; zhangyy@xzhmu.edu.cn

Introduction: Tumor vaccines can activate tumor-specific immune responses to inhibit tumor growth, recurrence, and metastasis. However, the efficiency of antigen and adjuvants combined delivery to lymph nodes (LNs) is relatively low, leading to weak immune stimulation and tolerance. In this study, a tumor nanovaccine was constructed for the targeted dendritic cells (DCs)-mediated immunotherapy.

Methods: Ovalbumin (OVA) antigen was first loaded into manganese-doped mesoporous silica nanoparticles (MMSNs) and coated with bacterial cytoplasmic membrane (BM), which was further inserted with mannose to prepare OVA@MMSNs@BM-Man nanovaccines. In vitro and in vivo experiments were conducted to assess their properties and function of the synthesized nanovaccines.

Results: The nanovaccine can effectively target DCs in LNs by the combination of mannose with mannose receptor (CD205). BM serves as an immune adjuvant and co-delivers with OVA antigen, effectively improving antigen presentation efficiency. In an acidic environment, the Mn^{2+} produced by the degradation of MMSNs can not only serve as an MR imaging agent but also activate the cGAS-STING pathway, followed by the release of IFN-β. The activated DCs further activate the body's cytotoxic T cells (CTLs), thereby exerting anti-tumor effects.

The conclusion: This study will provide a new idea for the construction of tumor nanovaccines.

Keywords: tumor nanovaccine, immunotherapy, cGAS-STING pathway, MR imaging

Introduction

Tumor subunit vaccines[1] have good stability, safety, and tolerance, which can activate the body's immune system by utilizing the specific function of antigen presenting cells (APCs), triggering the generation of antibodies and cytotoxic T cells (CTLs) to prevent and control the occurrence and development of tumors. Although subunit vaccines have great potential in cancer immunotherapy, the efficiency of antigen and adjuvants combined delivery to lymph nodes (LNs) is relatively low,[2,3] leading to weak immune stimulation and tolerance. In addition, in order to effectively induce CTLs mediated cellular immunity, antigens must enter APCs and then combine with major histocompatibility complex I (MHCI) to form molecular complexes, which bind to T cell receptors (TCRs) on the surface of T cells, inducing the production of antigen-specific CTLs and exerting anti-tumor effects.[4] Therefore, it is meaningful to construct a delivery system to deliver subunit vaccines to APCs in LNs.

Nanovaccines, which are composed of subunit vaccines and nanodelivery systems, have shown broad applications in the prevention and treatment of major diseases.[5–7] Compared with free subunit vaccines, nanovaccines have significant advantages: 1) protecting antigens from degradation and increasing stability;[8–10] 2) co-delivery of antigen and adjuvants

Received: 15 October 2024
Accepted: 6 February 2025
Published: 21 February 2025

Graphical Abstract

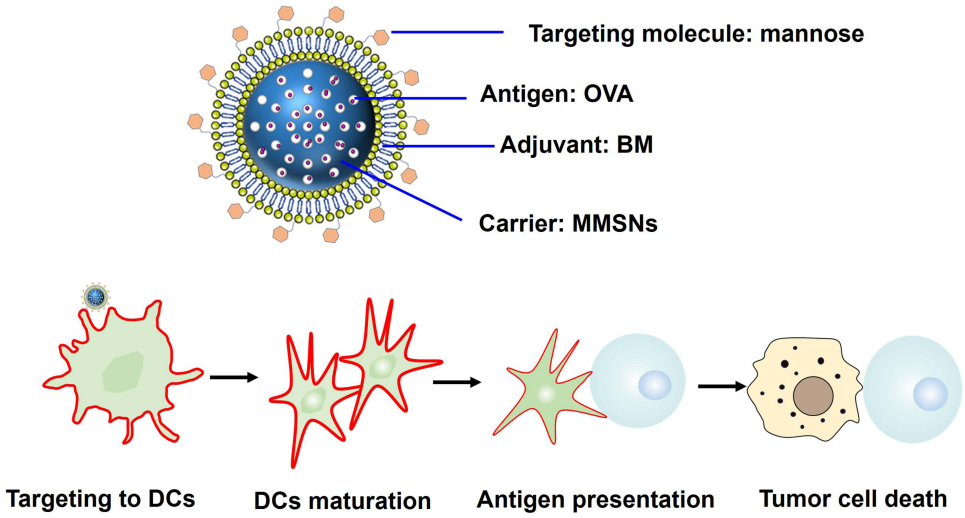

for synergistically activating APCs;[11,12] 3) nanocarriers with small size increasing the aggregation of antigens in LNs,[13] further enhancing the immune response.

Based on these advantages, manganese elements-doped mesoporous silica nanoparticles (MMSNs) with porous structure, pH-responsive degradation behavior and good biocompatibility can be used for antigen delivery.[14,15] In the degradation process of MMSNs, large amount of Mn^{2+} is released, which can not only be used for magnetic resonance (MR) imaging[16] but also for metal immunotherapy by the activation of cyclic GMP-AMP synthase (cGAS)-STING pathway in dendritic cells (DCs),[17,18] thus inducing the expression and secretion of type I interferon to enhance the immune responses. In addition, the co-delivery of antigen and immune adjuvants can induce a strong and persistent immune response. At present, many tumor nanovaccines composed of bacteria related substances have entered clinical trials.[19,20] In cancer vaccines, bacterial components can be used to enhance specific antitumor effects by promoting adaptive immune responses.[21,22] The bacterial cytoplasmic membranes (BM) do not contain toxic lipopolysaccharide (LPS) and other cell wall components,[23] which may be used as a potential adjuvant to reduce the toxic side effects.[24]

Herein, a tumor nanovaccine was constructed for the targeted DCs-mediated immunotherapy (Figure 1). Firstly, ovalbumin (OVA) antigen was loaded into MMSNs and coated with bacterial membrane (BM). Subsequently, mannose molecules were inserted into BM to prepare OVA@MMSNs@BM-Man nanovaccines, which can effectively target DCs by the combination of mannose with mannose receptor (CD205).[25] In an acidic lysosomal environment, MMSNs could degrade to release OVA antigen for antigen presentation. BM serves as an immune adjuvant and co-delivers with OVA antigen, effectively improving antigen presentation efficiency. In addition, the Mn^{2+} produced by the degradation of MMSNs can not only serve as an MR imaging agent to achieve delivery visualization but also activate the cGAS-STING pathway in DCs, followed by the release of IFN-β. The activated DCs further activate the body's CTLs, thereby exerting anti-tumor effects. Finally, a mouse melanoma model was used to investigate the immunotherapeutic efficacy of OVA@MMSNs@BM-Man nanovaccine. We hope this paper will provide a new idea for the construction of nanovaccines.

Material and Methods

Materials and Reagents

Triethanolamine (TEA), 3-aminopropyltriethoxysilane (APTES), hexadecyltrimethylammonium bromide (CTAB), hexadecyltrimethylammonium chloride (CTAC) and tetraethyl orthosilicate (TEOS) were purchased from Sigma-Aldrich

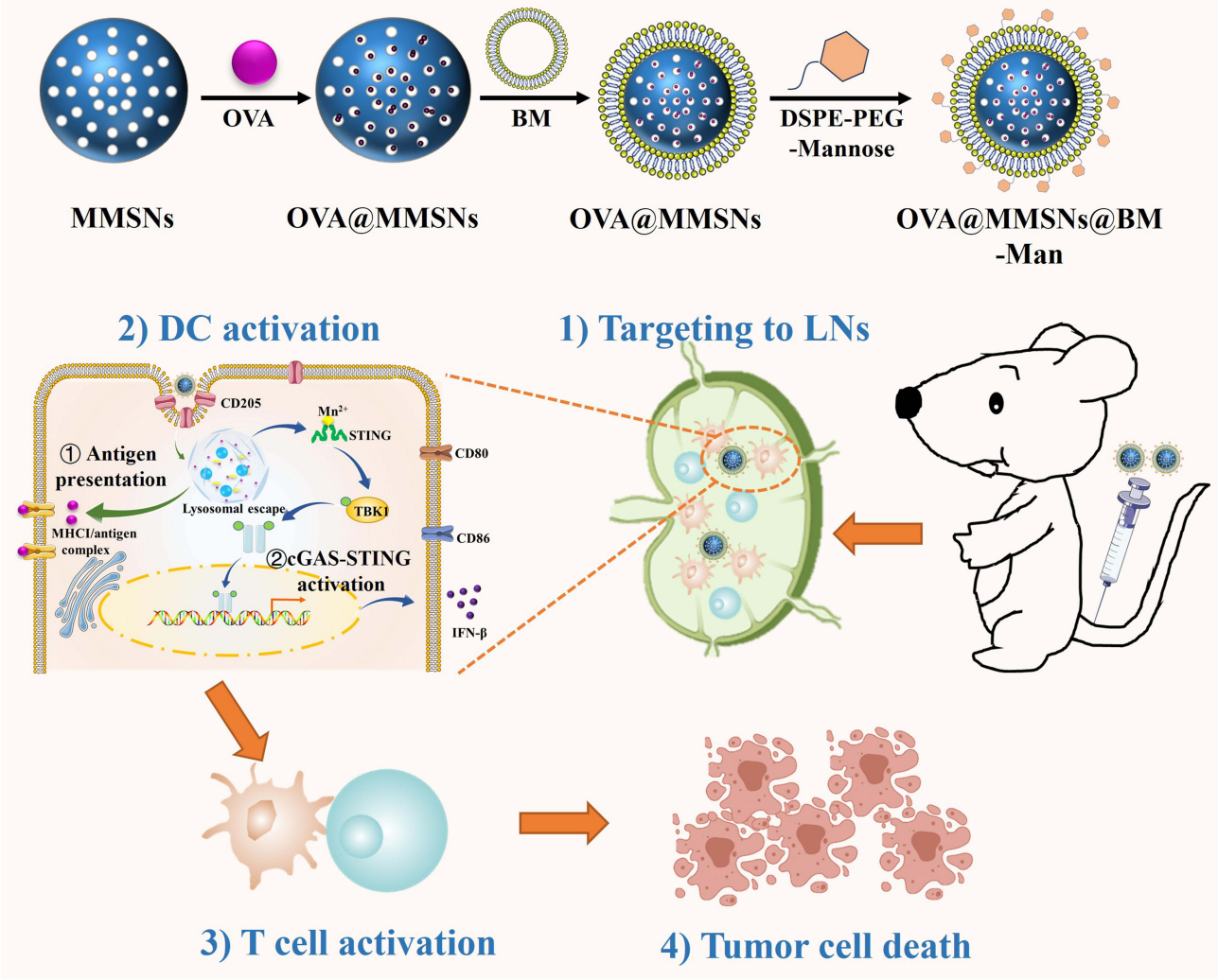

Figure 1 Schematic diagram of the preparation of OVA@MMSNs@BM-Man nanovaccine and its anti-tumor effects.

Chemical Reagent Co., Ltd (Shanghai, China). Ovalbumin (OVA) and manganese sulfate were bought from Macklin biochemical technology Co., Ltd (Shanghai, China). Fluorescein isothiocyanate labeled ovalbumin (FITC-OVA) and phospholipids-polyethylene glycol-mannose (DSPE-PEG-Mannose) were got from Xi'an ruixi Biological Technology Co., Ltd (China). PE anti-mouse CD11c, APC anti-mouse CD80, FITC anti-mouse CD86, APC anti-mouse CD8a, FITC anti-mouse CD4 and PE anti-mouse-CD3 antibodies were purchased from Elabscience. Reagents related to cell culture were obtained from GIBCO. Mouse IFN-β, TNF-α and IFN-γ enzyme linked immunosorbent assay (ELISA) kits were received from Jianglai Bio Co., Ltd (Shanghai, China).

Cells and Animals

Mouse dendritic cells (DC2.4s) were got from Shanghai Yu Bo Biotech Co., Ltd and cultured with RPMI-1640 medium +10% fetal bovine serum (FBS). Mouse melanoma cells modified with the OVA gene (B16-OVA) were purchased from Shanghai Mingjin Biotechnology Co., Ltd and cultured with RPMI-1640 medium+10% FBS+1% penicillin-streptomycin. All cells were cultivated in a 37°C, 5% CO_2 incubator.

C57/BJ6 female mice were purchased from GemPharmatech Co., Ltd (Nanjing, China) and cultured in accordance with the relevant standards of the Principles of Care for Experimental Animals. All animal experiments were approved

https://doi.org/10.2147/IJN.S496873

by the Animal Care Committee of Xuzhou Medical University and that the mice treatments were performed in compliance with the Guide for the Care and Use of Laboratory Animals.

Preparation of MMSNs Loaded With OVA (OVA@MMSNs)

First, MMSNs were synthesized according to the published literatures.[26] To load OVA, 5 mL of OVA solutions (40 mg/mL) were mixed and reacted with 20 mg of MMSNs for 24 h. After the reaction, solutions were centrifuged, washed and named as OVA@MMSNs.

Preparation of OVA@MMSNs@BM-Man Nanovaccine

First, the bacterial cytoplasmic membranes (BM) were extracted based on previous works.[24] The collected BMs were then mixed with OVA@MMSNs with a mass ratio of 1:1, followed by being sonicated at a frequency of 42 kHz for 20 min, and extruded by a liposome extruder back and forth 15–20 times to obtain BM coating OVA@MMSNs (OVA@MMSNs@BM). The obtained OVA@MMSNs@BM was reacted with 1 mg/mL of DSPE-PEG-Mannose at 37°C for 4 h, followed by centrifuging and washing to obtain OVA@MMSNs@BM-Man. In order to achieve the visual delivery of OVA, FITC-OVA was introduced, and the prepared products were named as FITC-OVA@MMSNs, FITC-OVA@MMSNs@BM and FITC-OVA@MMSNs@BM-Man.

Characterization

The morphologies were observed by transmission electron microscopy (TEM, FEI Tecnai G2 F30) equipped with energy-dispersive X-ray spectrum. The size distribution and surface zeta potentials were determined by a Zetasizer Nano ZS90 (Malvern Instruments, UK). The average pore diameter of MMSNs was measured by N_2 adsorption-desorption experiment. The fluorescence spectra were measured by fluorescence photometer (UH4150, HITACH). The coating of BM was verified by fluorescence co-localization assay.

The Magnetic Resonance (MR) Imaging Ability of MMSNs

Different concentrations of MMSNs (containing 0, 0.02, 0.04, 0.07, 0.13, 0.26, 0.31 and 0.64 mm of Mn^{2+}) were prepared under pH=7.4 and pH=5 conditions, and then MR imaging was performed using a 3.0 T GE Discovery 750W MR system. The scanning parameters were set as follows: repetition time (TR) = 3000 ms, echo time (TE) = 10 ms, field of view (FOV) = 18 cm×18 cm, slice thickness = 3.0 mm, spacing = 1.5 mm.

The Hemolysis Assay

Red blood cells (RBCs) were incubated with different concentrations of OVA@MMSNs@BM-Man (12.5 μg/mL, 25 μg/mL, 50 μg/mL, 100 μg/mL) at 37°C for 2 h. Among them, ddH_2O and PBS were set as positive and negative control groups, respectively. The absorbance of the supernatant at 541 nm was measured to calculate the hemolysis ratio.

The Cytotoxic Effects of OVA@MMSNs@BM-Man Nanovaccine

DC2.4s were incubated with different concentrations of OVA@MMSNs@BM-Man (6.25 μg/mL, 12.5 μg/mL, 25 μg/mL, 50 μg/mL, 100 μg/mL) for 24 h. Then 10 μL of CCK-8 was added to each well, and the absorbance value at 450 nm was measured to calculate the cell viability.

Cellular Uptake of OVA@MMSNs@BM-Man Nanovaccine

DC2.4s were cultured with FITC-OVA@MMSNs@BM-Man for 0 h, 1 h, 2 h, and 4 h, respectively. The cells were then washed and fixed with 4% paraformaldehyde for 10 min. After staining with 4', 6-diamino-2-phenylindole (DAPI), cells were imaged by a laser scanning confocal microscopy (CLSM, Leica STELLARIS 5, Germany). Similarly, cells with the treatments were subjected to flow cytometry (FACS Canto II) for quantitative analysis of cellular uptake efficiency.

Cellular MR Imaging

DC2.4s were cultured with OVA@MMSNs@BM-Man (containing 0.04 mm, 0.07 mm, 0.13 mm, and 0.26 mm of Mn elements) for 6 h. And then cells were collected and dispersed in 500 μL of PBS for MR imaging using a 3.0 T GE

Discovery 750W MR system. The scanning parameters were set as follows: repetition time (TR) = 3000 ms, echo time (TE) = 10 ms, field of view (FOV) = 18 cm×18 cm, slice thickness = 3.0 mm, spacing = 1.5 mm.

In Vitro Activation of DC2.4 Cells

DC2.4s were cultured with OVA, MMSNs, OVA@MMSNs, OVA@MMSNs@BM and OVA@MMSNs@BM-Man for 6 h. In addition, the contents of OVA in OVA, OVA@MMSNs@BM and OVA@MMSNs@BM-Man groups were 20 μg/mL. After washing with PBS, cells were digested, collected, washed and cultured with anti-CD11c-PE, anti-CD80-APC, and anti-CD86-FITC antibodies in dark for 30 min. The cells were then centrifuged and dispersed for flow cytometric analysis (FACS Canton II).

The Activation of cGAS-STING Pathway by Mn^{2+} in DC2.4s

DC2.4s were cultured with OVA, MMSNs, OVA@MMSNs, OVA@MMSNs@BM and OVA@MMSNs@BM-Man for 6 h. In addition, the contents of OVA in OVA, OVA@MMSNs@BM and OVA@MMSNs@BM-Man groups were 20 μg/mL. Then, the cell supernatants were collected for the measurement of IFN-β by ELISA kits according to the manufacturer's instructions.

MR Imaging of Mouse LNs

One hundred microliter of PBS, OVA@MMSNs@BM and OVA@MMSNs@BM-Man (5 mg/kg) were subcutaneously injected into the root of the tail. After 12 h, mice were sacrificed, and LNs were collected and grinded to prepare cell suspensions, which were centrifuged at 2500 rpm for 10 min, and then cell precipitates were fixed with 4% paraformaldehyde for 10 min, redistributed in 0.5% agarose gel solution for MR imaging using a 3.0 T GE Discovery 750W MR system, and the T_1WI signal intensity was also measured.

In Vivo Anti-Tumor Effects

To establish subcutaneous melanoma model, 5×10^5 cells/mouse of B16-OVA cells were subcutaneously injected into the right hind legs. About 7 days later, tumor bearing mice were randomly divided into six groups: PBS, OVA, MMSNs, OVA@MMSNs, OVA@MMSNs@BM, OVA@MMSNs@BM-Man. All formulations (200 μL, 5 mg/kg) were subcutaneously injected at the base of mouse tail. During the treatment, the tumor size and body weight changes were recorded every 2 days. The survival time of mice in each group was also recorded.

In Vivo Immune Cell Activation

After the treatment, LNs were removed, grinded, rinsed with PBS buffer, and centrifuged at 2500 rpm for 7 min to obtain the precipitates. Afterwards, 2.5 μL of anti-CD11c-PE, anti-CD80-APC, and anti-CD86-FITC antibodies were added and incubated at room temperature in dark for 30 min. After centrifuging at 2000 rpm for 7 min, cell precipitates were mixed with 4% paraformaldehyde solution, and subjected to flow cytometry (FACS Canto II) to analyze the activation of DCs.

Similarly, tumor cells were incubated with 5 μL of anti-CD8a-APC, anti-CD4-FITC, and anti-CD3-PE antibodies at room temperature in the dark for 30 min. The cells were then subjected to flow cytometry (FACS Canto II) to detect the changes of CTLs ($CD3^+CD4^-CD8^+$T) proportion.

Measurement of Immune Factors

After the treatment, LNs were collected, grinded, rinsed with PBS buffer, and centrifuged at 2500 rpm for 7 min to obtain the supernatants. The concentrations of IFN-β in the supernatants were measured using ELISA kits. At the same time, blood was collected, and the concentrations of serum TNF-α and IFN-γ were measured by ELISA kits.

In Vivo Biosafety

Mouse Blood Routine and Biochemical Analysis

Two hundred microliters of OVA@MMSNs@BM-Man solution (5 mg/kg) was injected to C57-BJ6 mice through tail vein. Blood was collected on the 1st, 7th, and 21st day after injection for blood routine and biochemical tests.

Pathological Sections of Main Organs

C57-BJ6 mice with the same treatments were euthanized on the 1st, 7th, and 21st day after injection. Heart, liver, spleen, lung, and kidney tissues were taken and fixed with 4% paraformaldehyde for hematoxylin eosin (HE) staining.

MR Metabolic Imaging

C57-BJ6 female mice were intravenously injected with 200 μL of OVA@MMSNs@BM-Man biomimetic nanovaccine (containing 2.5 mm of Mn element). After injection for 0.5 h, 1 h, 2 h, 4 h, 6 h, 8 h, 10 h, and 24 h, mice were anesthetized and fixed for MR imaging using a 3.0 T GE Discovery 750W MR system. The MR imaging scanning sequence in mice was performed using Gradient Echo (GRE) sequence with scanning parameters of TR=16 ms, TE=3.2 ms, FOV=8 cm × 8 cm, matrix=320 × 288, layer thickness=1.0 mm, and interlayer spacing=0.5 mm.

Data Analysis

The experimental results were expressed as mean ± standard deviation (Mean ± SD). All data processing was carried out on GraphPad Prism software. Data analysis was performed using *t*-test and one-way Analysis of Variance (ANOVA) method. Values of P <0.05 were statistically significant (*$P < 0.05$, **$P < 0.01$).

Results

Characterization of OVA@MMSNs@BM-Man Nanovaccine

In this paper, MMSNs were prepared by an in-situ preparation method,[27] which were used for subsequent co-delivery of antigens and immune adjuvants. TEM images of MMSNs and OVA@MMSNs@BM-Man were shown in Figure 2A. MMSNs exhibited a spherical and mesoporous structure with good monodispersity. Then a layer of cell membrane structure was coated on the surface of MMSNs as seen in the TEM image of OVA@MMSNs@BM-Man. Subsequently, the mesoporous structure of MMSNs was validated through N_2 adsorption-desorption assay (Figure S1), which had a mesoporous structure with a specific surface area, pore volume, and pore size of 719.70 g/m^2 and 1.22 cm^3/g and 5.64 nm, respectively. In order to further verify the successful doping of manganese elements into MSNs, elemental and spectral analysis were conducted in Figure 2B and C. Carbon, silicon, oxygen, and manganese elements were found in MMSNs, indicating that manganese elements had been successfully incorporated into MSNs.

Subsequently, dynamic light scattering (DLS) method was used to analyze the hydratization size and potential charges of nanovaccines. As displayed in Figure 2D, the particle sizes of MMSNs, OVA@MMSNs, OVA@MMSNs@BM and OVA@MMSNs@BM-Man were approximately 164, 164, 190, and 220 nm. After the encapsulation of BM and the modification of mannose molecules, the particle size of OVA@MMSNs slightly increased. In addition, the surface zeta potentials of different nanoparticles in the preparation process of OVA@MMSNs@BM-Man were also tested. After the loading of OVA antigen, the zeta potential of MMSNs changed from −19.27 mV to −13.23 mV (Figure 2E). With the modification of BM and mannose, the negative charges of OVA@MMSNs@BM and OVA@MMSNs@BM-Man were −20.97 mV and −13.03 mV, respectively.

The Verification of OVA Loading and BM Encapsulation

In order to verify whether OVA antigen was successfully loaded into MMSNs, the fluorescence spectra of FITC-OVA and FITC-OVA@MMSNs@BM-Man were shown in Figure 2F. Both FITC-OVA and FITC-OVA@MMSNs@BM-Man had characteristic fluorescence absorption peaks at 520 nm, while MMSNs had no fluorescence absorption peak at 520 nm, indicating that FITC-OVA had been successfully loaded into MMSNs.

Subsequently, an inverted fluorescence microscope was used to observe the fluorescence co-localization effect. As shown in Figure 2G, the green fluorescence of FITC-OVA was mostly overlapped with the red fluorescence of BM-DID, indicating the successful loading of FITC-OVA and encapsulation of BM in FITC-OVA@MMSNs@BM-Man.

All the above data indicated the successful synthesis of MMSNs, loading of OVA, and encapsulation of BM, demonstrating the successful preparation of OVA@MMSNs@BM-Man nanovaccine, which had laid the foundation for functional verification.

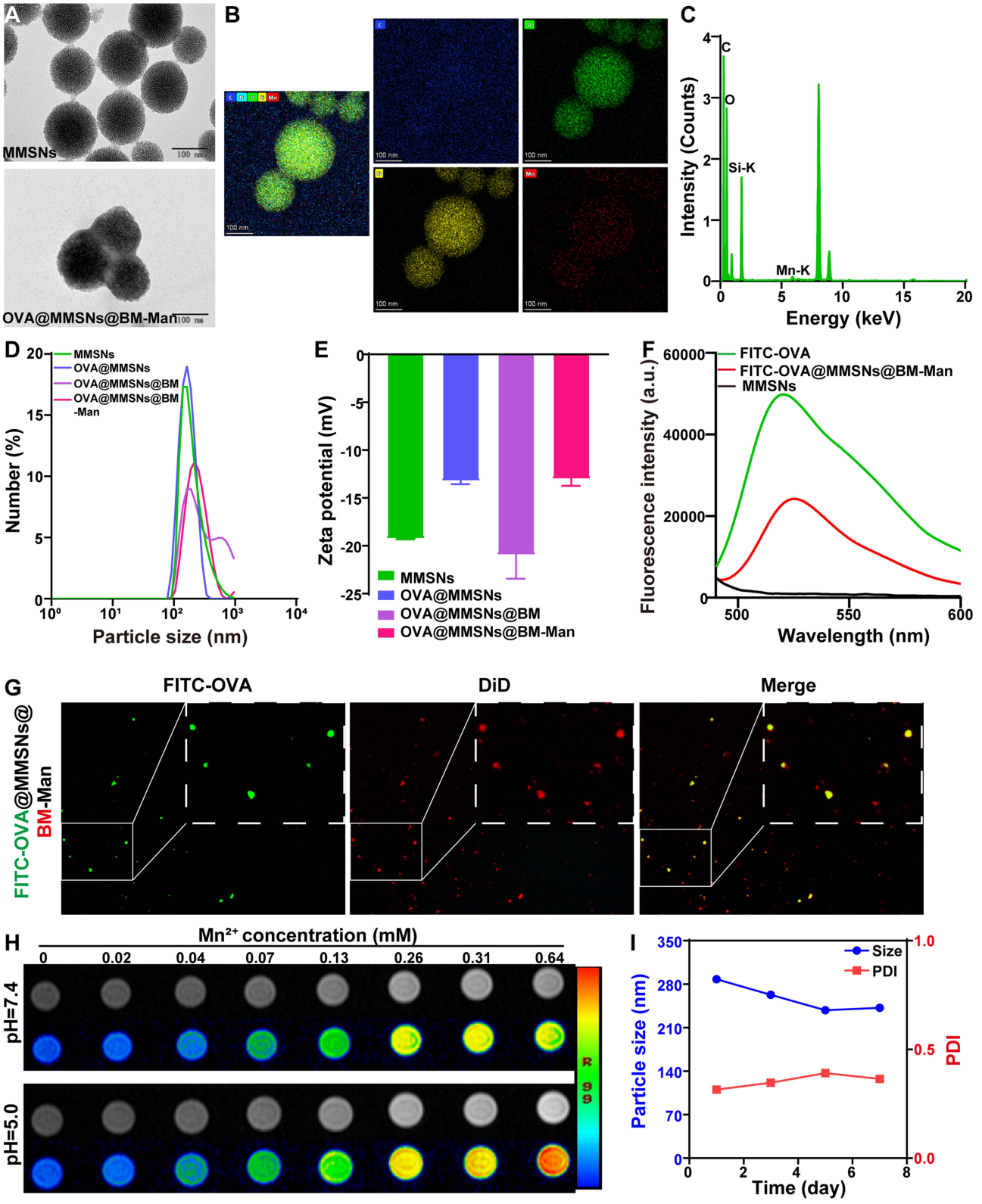

Figure 2 Characterization of OVA@MMSNs@BM-Man. (**A**) TEM images of MMSNs and OVA@MMSNs@BM-Man; (**B**) Elemental mapping analysis of MMSNs; (**C**) Energy spectrum analysis; (**D**) Size distribution of OVA@MMSNs@BM-Man; (**E**) Changes of surface zeta potentials; (**F**) Fluorescence spectra of FITC-OVA, MMSNs and FITC-OVA @MMSNs@BM-Man; (**G**) Fluorescence co localization experiment (green: FITC-OVA; red: DiD labelled BM); (**H**) T_1 MR images of OVA@MMSNs@BM-Man with different Mn contents in pH5.0/7.4 solutions; (**I**) Changes of size and PDI during the storage at 4°C for one week.

https://doi.org/10.2147/IJN.S496873

The MR Imaging Ability

As we know, MMSNs possess a pH-responsive degradation behavior and the generation of Mn^{2+} can be used for MR imaging.[28,29] As displayed in Figures 2H and S2, the T_1WI signal value in ROI region increased as the concentration of Mn^{2+} increased, and the pseudocolor image gradually changed from blue to red, confirming that the T_1WI signal values of MMSNs were concentration-dependent. In addition, the T_1WI signal value of MMSNs at the same Mn^{2+} concentration in pH5.0 was higher than that in pH7.4, which was mainly due to the degradation of MMSNs in pH5.0, releasing more Mn^{2+} for MR imaging. The pH-responsive MR imaging ability made MMSNs suitable for visualizing in vivo delivery.

The Stability Assessment

In the field of biomedical science, stability is a key factor in determining whether nanomedicines can achieve their expected functions in vivo. To verify the stability, OVA@MMSNs@BM-Man was dispersed in PBS solution and stored at 4°C for 7 days. The changes in particle size and polydispersity index (PDI) were measured using the DLS method. The particle size of OVA@MMSNs@BM-Man was relatively constant, and the PDI was always less than 0.5 (Figure 2I). At the same time, the solution had been in a clear and transparent state without significant precipitation, indicating that OVA@MMSNs@BM-Man was less prone to agglomeration at 4°C, making it easier to store.

In Vitro Biosafety

Before evaluating the efficacy of nanovaccines, their biological safety should be first evaluated. The in vitro biosafety of OVA@MMSNs@BM-Man was verified by hemolysis and cytotoxicity experiments. In the RBC hemolysis experiment, compared with the ddH_2O group, there was no significant hemolysis observed in PBS and OVA@MMSNs@BM-Man groups. In addition, the hemolysis rate was still below 6% even at a concentration of 100 μg/mL (Figure 3A).

Subsequently, the cytotoxicity of OVA@MMSNs@BM-Man on DC2.4s was evaluated by CCK-8 assay. The cell viabilities of DC2.4s were always higher than 85% in the concentration range of 0–100 μg/mL (Figure 3B). Although the cell survival rate slightly decreased with the increase in concentration, the cell viability of DC2.4s at the highest concentration (100 μg/mL) was still as high as 89.88%, indicating that OVA@MMSNs@BM-Man nanovaccine had good biocompatibility against DC2.4s.

Both the RBCs hemolysis and CCK-8 experiments verified the good biosafety of OVA@MMSNs@BM-Man nanovaccine, laying the foundation for subsequent functional verification experiment.

Cellular Uptake

The internalization of nanovaccines is a key step for achieving therapeutic effects. First, flow cytometry was used to quantitatively analyze the cellular uptake effects of FITC-OVA@MMSNs@BM-Man in DC2.4s. With the prolongation of incubation time, the green fluorescence intensity inside DC2.4s increased. After 1 h, 2 h and 4 h of incubation, the proportions of FITC-OVA positive DC2.4s were 8.89%, 21.97%, and 25.86%, respectively (Figure 3C and D). Among them, the fluorescence intensity at 4 h was slightly higher than that at 2 h, indicating that the cellular uptake basically reached saturation at 2 h.

Subsequently, CLSM was used for the qualitative observation of cellular uptake of nanovaccines by DC2.4s. After co-culturing with nanovaccines for 0.5 h, slight green fluorescence appeared in the cytoplasmic region of DC2.4s, confirming that the nanovaccine had begun to partially enter the cytoplasm (Figures 3E and S3). As the co-incubation time increased, the green fluorescence intensity gradually increased, indicating a sustained uptake of nanovaccines by DC2.4s.

Cellular MR Imaging

According to published works, Mn^{2+} can be used for T_1 MR imaging. To verify whether MMSNs could be degraded in DC2.4s, the cellular MR imaging was conducted. As shown in Figures 3F and S4, as the concentration of Mn^{2+} increased, the T_1WI signal value of DC2.4s increased, and the pseudocolor of cells changed from blue to red. Quantitative measurement of signal values proved that the cellular MR imaging of DC2.4s was concentration dependent.

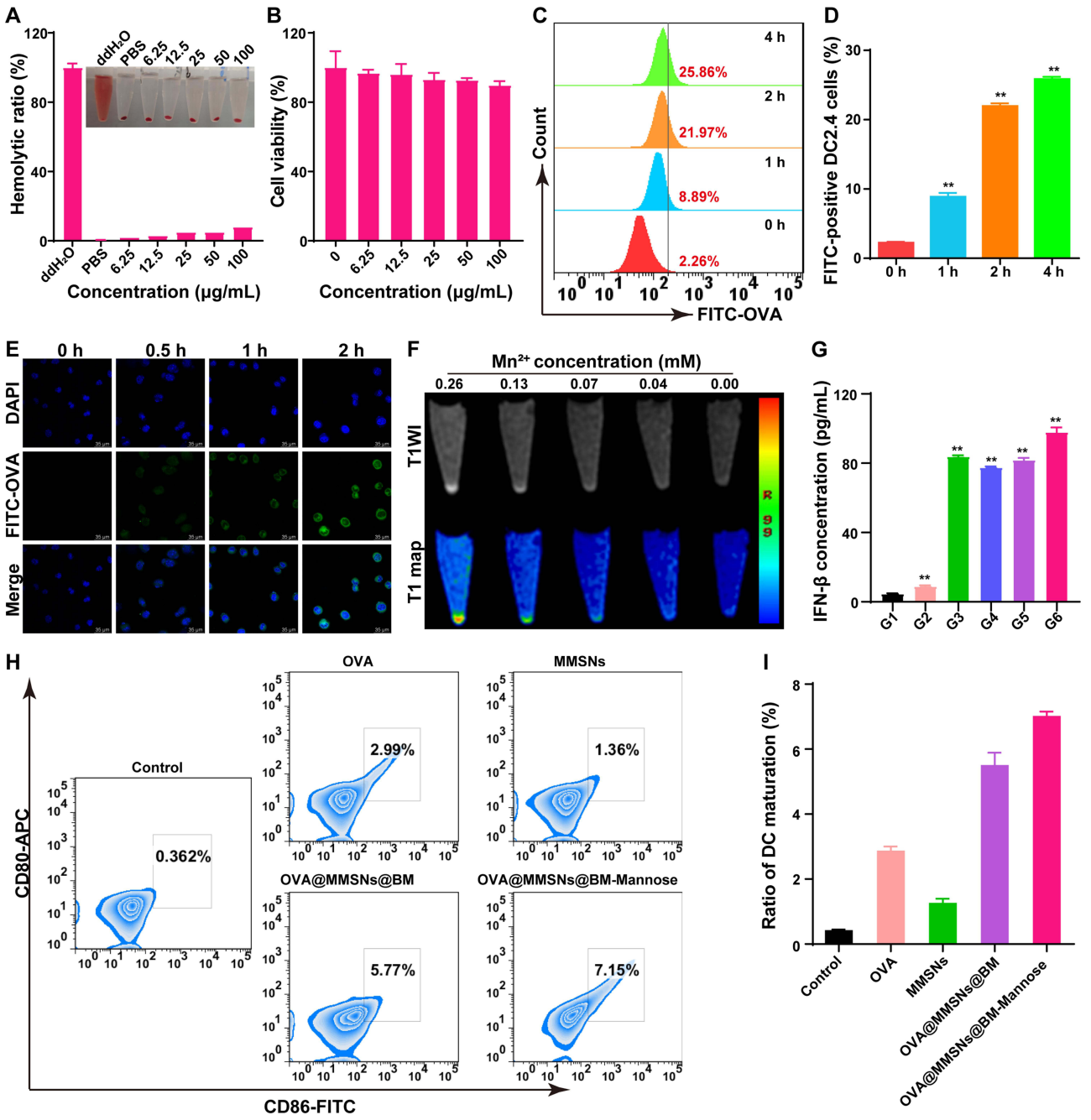

Figure 3 In vitro test of cellular targeting ability and DC maturation. (**A**) Hemolysis test of RBCs incubation with different concentrations of OVA@MMSNs@BM-Man; (**B**) Cell viabilities of DC2.4 cells cultured with different concentrations of OVA@MMSNs@BM-Man; (**C**) Flow cytometric of DC2.4 cells incubation with FITC-OVA @MMSNs@BM-Man for 1, 2 and 4 h, respectively; (**D**) Quantitative analysis of FITC-OVA positive DC2.4 cells; (**E**) Confocal images of DC2.4 cells incubation with FITC-OVA@MMSNs@BM-Man for 0.5, 1 and 2 h; (**F**) T_1 MR images of DC2.4 cells incubation with different Mn contents of OVA@MMSNs@BM-Man for 2 h; (**G**) Measurement of IFN-β in the supernatants of DC2.4s (G1: Control; G2: OVA; G3: MMSNs; G4: OVA@MMSNs; G5: OVA@MMSNs@BM; G6: OVA@MMSNs@BM-Man); (**H** and **I**): Flow cytometric and quantitative analysis of DC maturation. $^{**}P<0.01$, compared with control group.

The above assays proved that OVA@MMSNs@BM-Man nanovaccine could be uptaken by DC2.4 cells and degraded into Mn^{2+} for MR imaging. These results further indicated that the degradation of MMSNs could induce the release of OVA antigen and BM adjuvant for subsequent antigen presentation.

The Activation of cGAS-STING Pathway by Mn^{2+}

Due to the degradation of MMSNs within DCs, a large amount of Mn^{2+} was generated. Researches have shown that Mn^{2+} can activate the cGAS-STING pathway, promote the secretion of type I interferon, and thus activate the body's immune

https://doi.org/10.2147/IJN.S496873

system. To verify whether the released Mn^{2+} promoted the secretion of IFN-β, the changes of IFN-β in the cell supernatant were detected using an ELISA kit. The concentrations of IFN-β in Control, OVA, MMSNs, OVA@MMSNs, OVA@MMSNs@BM and OVA@MMSNs@BM-Man groups were 4.68 pg/mL, 8.96 pg/mL, 83.85 pg/mL, 77.60 pg/mL, 81.81 pg/mL, and 97.95 pg/mL, respectively (Figure 3G). Among them, OVA@MMSNs@BM-Man group had a higher IFN-β content than OVA@MMSNs@BM group, which was mainly due to the targeted delivery effect mediated by mannose, more OVA@MMSNs@BM-Man nanoparticles entered the cells.

In Vitro Activation of DC2.4s

After the uptake of OVA@MMSNs@BM-Man nanovaccine, the released OVA and BM separately act as antigen and immune adjuvant to activate DCs. As shown in Figure 3H and I, the ratios of mature DC2.4s in MMSNs group were 1.36%, which was higher than that in control group (0.36%). This was due to the role of Mn^{2+} as an immune adjuvant. While OVA, OVA@MMSNs@BM and OVA@MMSNs@BM-Man groups had 2.99%, 5.77%, and 7.15% of mature DC2.4s, respectively. In addition, the ratio of mature DC2.4s in OVA@MMSNs@BM-Man group was higher than that in OVA@MMSNs and OVA@MMSNs@BM groups, which was attributed to the synergistic effect of the targeting ability of mannose and the co-delivery of OVA antigen and BM adjuvant.

The MR Imaging of LNs

B16-OVA tumor bearing mice were used to evaluate the therapeutic effect of OVA@MMSNs@BM-Man nanovaccine. The schedule of animal experiments was shown in Figure 4A. In order to verify the targeted delivery of nanovaccines to LNs, T_1WI and pseudocolor images were obtained after injection of OVA@MMSNs@BM and OVA@MMSNs@BM-Man (Figure 4B and C). The MR signals in OVA@MMSNs@BM and OVA@MMSNs@BM-Man groups were significantly higher than that in control group. In addition, the LNs signal intensity in OVA@MMSNs@BM group was significantly lower than that in OVA@MMSNs@BM-Man group, confirming that the addition of mannose molecules could enhance the delivery efficiency to LNs.

In Vivo Anti-Tumor Effects

During the treatment period, there was no significant weight loss in each group of mice (Figure 4D), indicating that the nanovaccine had good biological safety. After treatment, the tumor volumes in PBS, OVA, MMSNs, OVA@MMSNs, OVA@MMSNs@BM and OVA@MMSNs@BM-Man groups were 1485.8 mm^3, 1033.4 mm^3, 1380.3 mm^3, 964.5 mm^3, 556.0 mm^3, and 370.1 mm^3, respectively (Figure 4E and F). The tumor inhibition rates in OVA, MMSNs, OVA@MMSNs, OVA@MMSNs@BM and OVA@MMSNs@BM-Man groups were 30.4%, 19.89%, 35.1%, 62.6%, and 75.1%, respectively (Figure 4G). In addition, OVA@MMSNs@BM-Man group had the smallest tumor volume and the highest inhibition rate, indicating that OVA@MMSNs@BM-Man nanovaccine could effectively inhibit tumor growth. In addition, 2 of 5 mice in PBS group died on the 13^{th} day after injection, and 1 of 5 mice in OVA, MMSNs, OVA@MMSNs or OVA@MMSNs@BM died on the 15^{th} day, while no mice in OVA@MMSNs@BM-Man group died during the treatment period (Figure 4H). These data demonstrated that OVA@MMSNs@BM-Man could not only inhibit tumor growth but also extend the survival time of mice.

Immune Cell Activation Analysis

Related works have reported that the combination of OVA and Mn^{2+} could effectively activate DCs and T cells.[30] In order to verify the activation effect of DCs, LNs were collected for flow cytometric analysis. As shown in Figure 5A and B, PBS (0.088%) and MMSNs groups (0.308%) had low DCs activation efficiency, while the ratios of mature DCs in OVA, OVA@MMSNs, OVA@MMSNs@BM and OVA@MMSNs@BM-Man groups were 2.92%, 3.99%, 6.68%, and 9.38%, respectively. In addition, OVA@MMSNs@BM-Man group had the highest ratio of mature DCs, which was beneficial from the targeted delivery of antigen and adjuvant.

Subsequently, the activation of cGAS-STING pathway in DCs was verified by ELISA assay. As illustrated in Figure 5C, the IFN-β concentrations in PBS, OVA, MMSNs, OVA@MMSNs, OVA@MMSNs@BM and OVA@MMSNs@BM-Man groups were 0.75, 0.53, 1.60, 1.72, 2.14 and 9.52 pg/mL. In addition, OVA@MMSNs@BM-

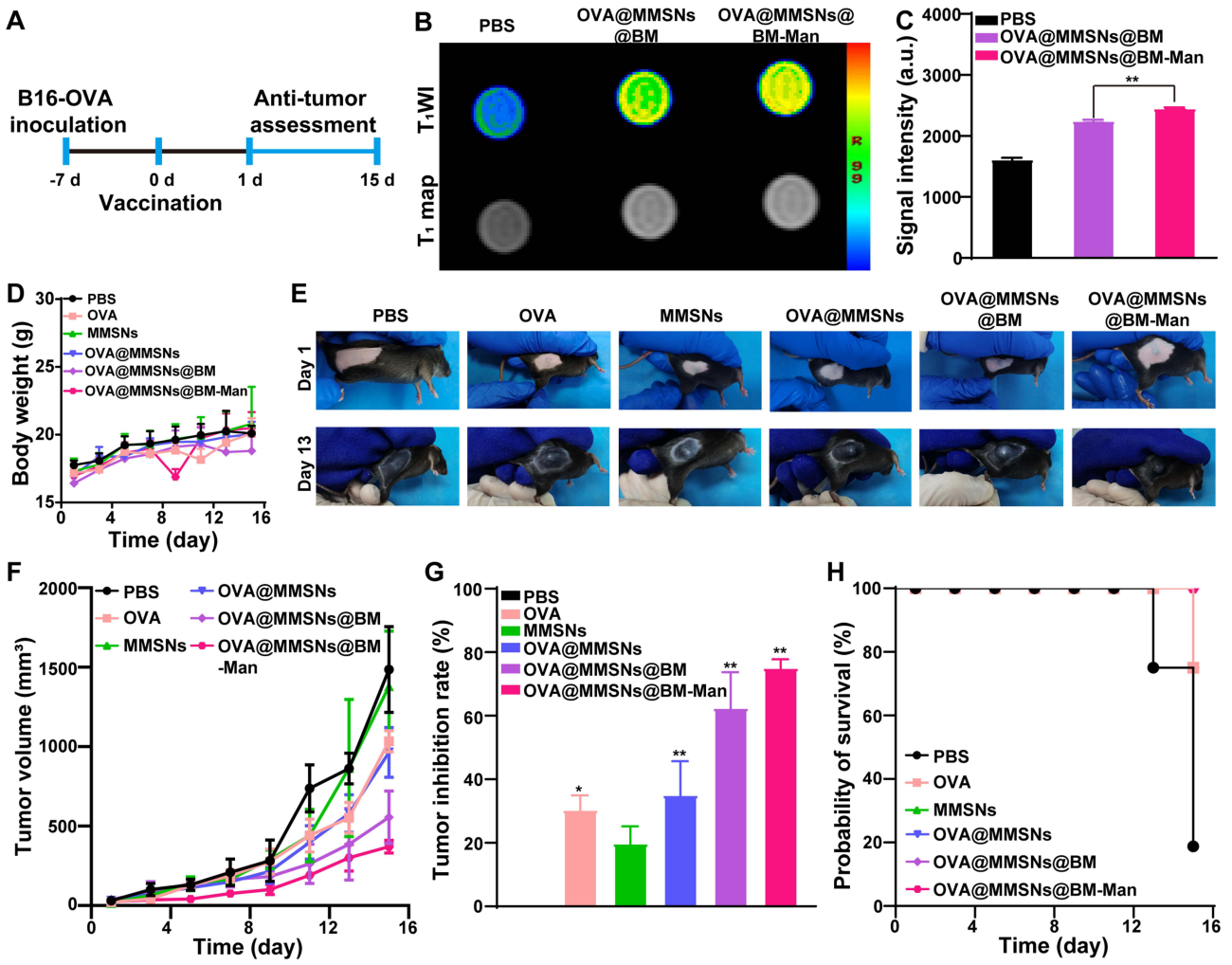

Figure 4 In vivo anti-tumor effects. (**A**) Schedule of animal experiments; (**B**) MR images of LNs cell suspension of different groups to measure the targeting ability of OVA@MMSNs@BM-Man nanovaccine; (**C**) Quantitative analysis of MR signal intensities; ***P*<0.01, compared with OVA@MMSNs@BM group; (**D**) Body weight changes of mice during the treatment; (**E**) Representative images of tumor bearing mice; (**F**) Tumor volume change curves; (**G**) Tumor inhibition rates in all groups; **P*<0.05, ***P*<0.01, compared with control group; (**H**) Survival rates of mice in different groups.

Man group displayed the highest IFN-β content, which was 12.7-fold to that in PBS group. These results indicated that MMSNs could degrade and release Mn^{2+} to activate the cGAS-STING pathway, thus inducing the generation and secretion of type I interferon.

In addition, the activation of DCs could further activate CTLs. Therefore, the generation of CTLs is a key factor in measuring the effectiveness of tumor nanovaccines. Changes of CTLs proportion in tumor tissues were detected by flow cytometry. As shown in Figure 5D and E, the ratios of CTLs ($CD3^+CD4^-CD8^+$) in PBS and MMSNs groups were 2.27% and 2.54%, which were lower than that in OVA (3.28%), OVA@MMSNs (4.06%), OVA@MMSNs@BM (4.12%) and OVA@MMSNs@BM-Man (5.45%) groups, respectively. Among them, OVA@MMSNs@BM-Man group displayed the highest percentage of CTLs, indicating that it could activate DCs, thus increasing the percentage of tumor infiltrating CTLs to exert tumor killing effects. These data indicated that the combination of Mn^{2+}, OVA and BM could effectively induce the generation of CTLs.

Immune Factors Analysis

During the treatment process, the generation of immune factors is a key factor in evaluating the effectiveness of immune activation. To further investigate the immune response after various therapies, the serum cytokines (TNF-α and IFN-γ) were evaluated by ELISA. TNF-α, as a tumor killer, is mainly secreted by activated T lymphocytes to induce cancer cell

https://doi.org/10.2147/IJN.S496873

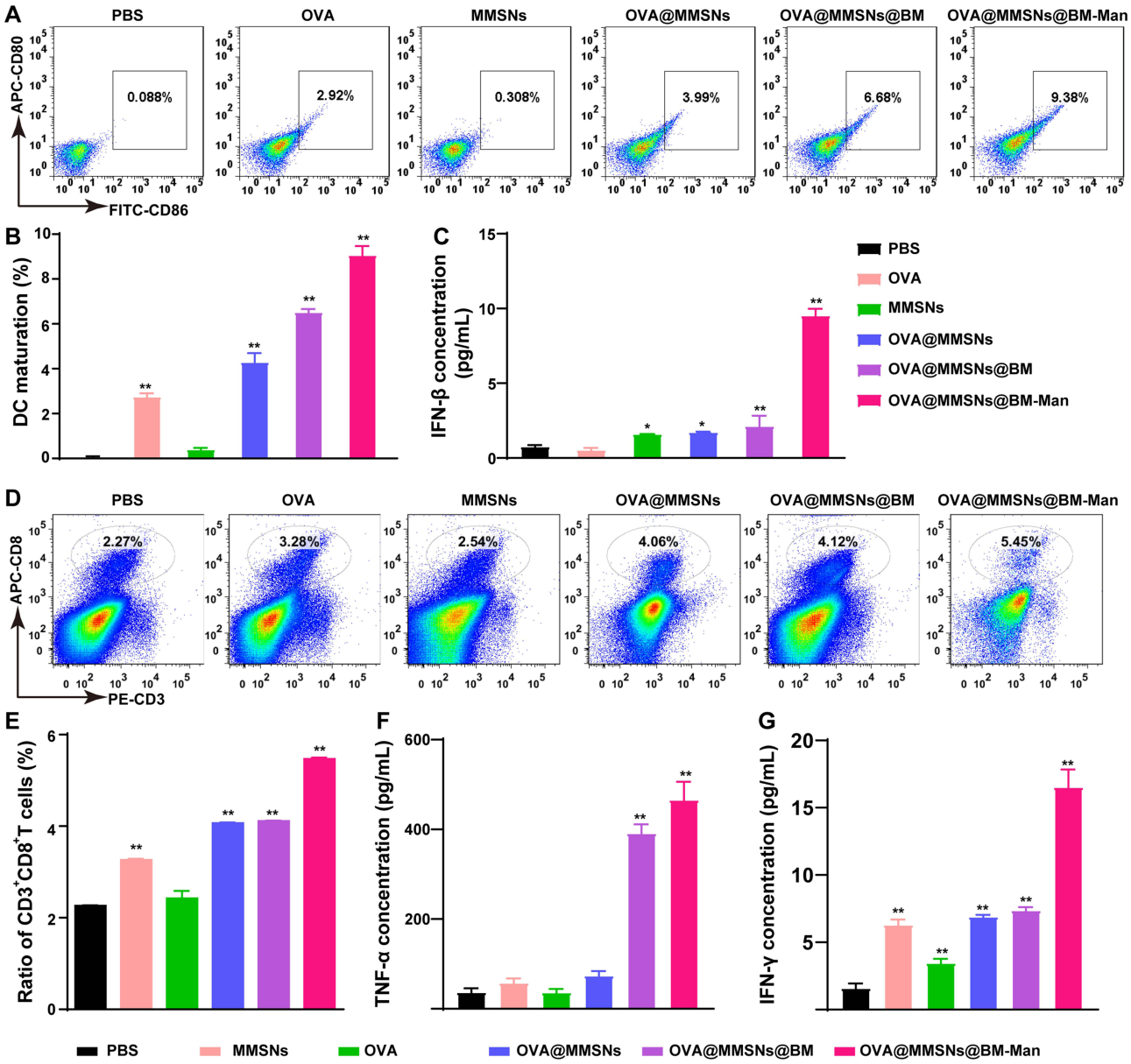

Figure 5 Immune cell activation analysis. (**A**) Flow cytometric analysis of DCs maturation in LNs; (**B**) Quantitative analysis of mature DCs; (**C**) Measurement of IFN-β in LNs; (**D**) Analysis of CTLs ratios by flow cytometry; (**E**) Quantitative analysis of CTLs percentages; ELISA measurements of serum TNF-α (**F**) and IFN-γ (**G**) contents in different groups. *P<0.05, **P<0.01, compared with PBS group.

apoptosis.[31] IFN-γ is a key cytokine related to antitumor immunity, which protects the body by exerting cell inhibitory function, promoting cancer cell apoptosis, and immune stimulation.[32] As shown in Figure 5F, the contents of TNF-α in OVA, MMSNs and OVA@MMSNs groups were slightly higher than that in control group. In addition, the TNF-α concentration in OVA@MMSNs@BM-Man group was significantly higher than OVA@MMSNs@BM group, which was consistent with the above results. Excitingly, the changes of IFN-γ (Figure 5G) concentrations were similar to TNF-α. The measurement of immune cytokines demonstrated that the nanovaccine could kill tumor cells and effectively activate the host immunity.

In Vivo Biocompatibility

After the injection of OVA@MMSNs@BM-Man, blood samples were collected at different time points for routine and biochemical tests to evaluate the in vivo toxicity. As shown in Figure 6A and B, compared with control group,

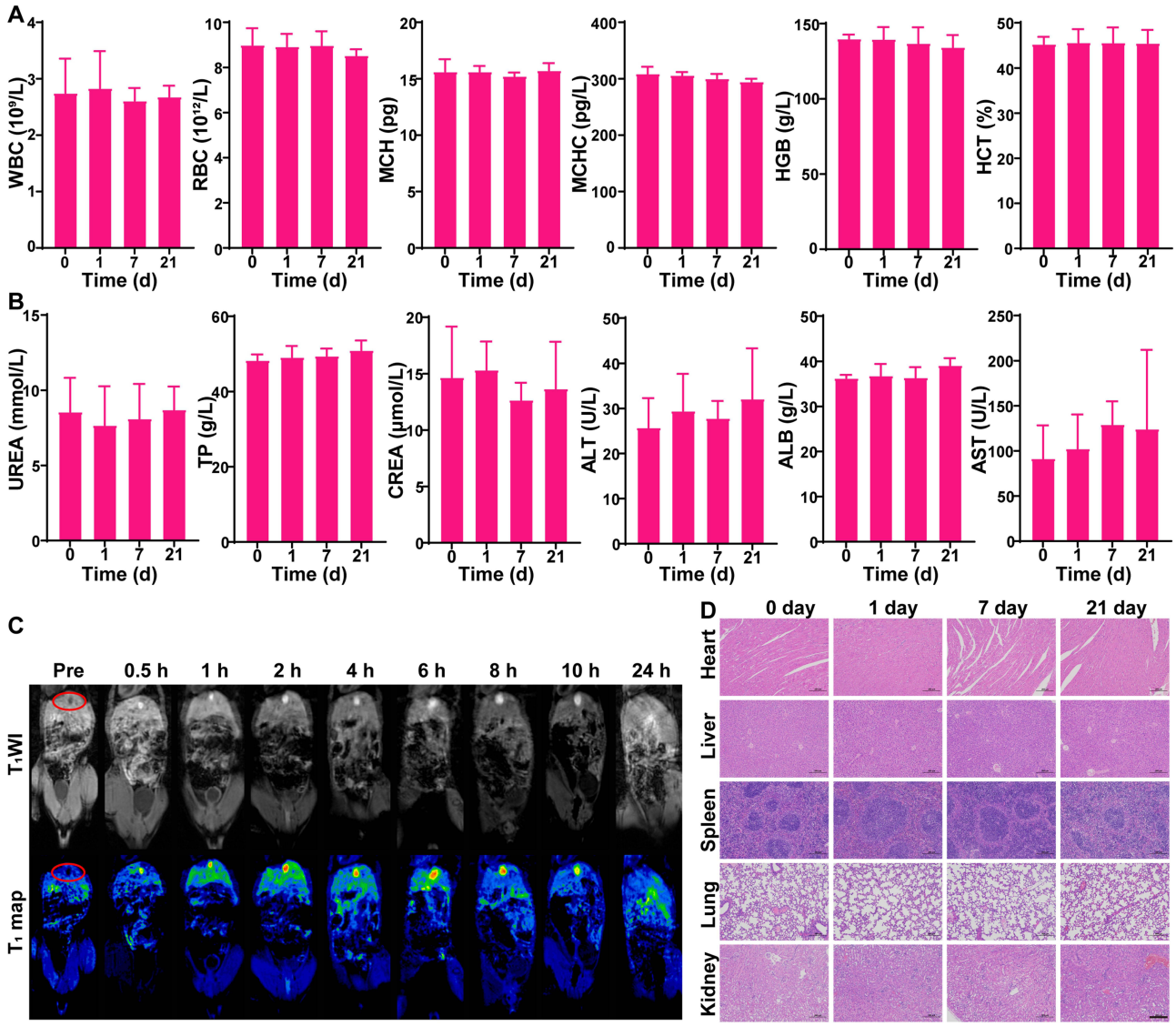

Figure 6 In vivo biosafety of OVA@MMSNs@BM-Man nanovaccine. (**A**) Blood routine analysis after 1, 7, 21 days' injection of OVA@MMSNs@BM-Man nanovaccine; (**B**) Blood biochemistry analysis; (**C**) Metabolism analysis by MR imaging (The red circle represents the metabolic region); (**D**) HE staining of main organs (scale bar: 200 μm).

there was no significant difference in various hematological indicators of OVA@MMSNs@BM-Man mice, confirming that the nanovaccine did not show significant toxicity to mice at the experimental dose. In addition, OVA@MMSNs@BM-Man nanovaccine was metabolized through the gallbladder of mice, which did not show any enhanced shadows in kidneys and bladder during the entire metabolic process (Figure 6C), indicating that OVA@MMSNs@BM-Man was metabolized through the liver and gallbladder system. Furthermore, there was no significant enhancement in the gallbladder area of mice after 24 h, confirming that the nanovaccine could be metabolized completely in mice within 24 hours without any biological accumulation occurring in the body. In addition, HE staining results indicated that all organs showed no significant organic lesions, inflammation, or other abnormalities (Figure 6D).

Discussion

Tumor vaccines activate the body's immune system by injecting tumor associated antigens or tumor-specific antigens into the patient's body, thereby achieving the goal of controlling or clearing tumors.[33] At present, there are four tumor vaccines on the market, such as human papillomavirus (HPV) vaccine, hepatitis B vaccine, prostate cancer therapeutic vaccine and

https://doi.org/10.2147/IJN.S496873

lung cancer therapeutic vaccine. The main mechanism of tumor vaccines is to use the specific function of professional APCs to trigger helper T cell responses, support antibody production, and induce the production of CTLs, thereby exerting anti-tumor effects. Therefore, how to effectively promote the generation of CTLs has become a key factor in tumor vaccine development. However, tumor vaccines have problems such as low lymph node drainage efficiency and poor stability, leading to poor anti-tumor effects. This study constructed MMSNs for loading OVA antigen, subsequently coated with bacterial membranes as immune adjuvants to enhance immune responses. Finally, mannose molecules were inserted onto the surface of BM to target DCs and achieve targeted immunotherapy for melanoma.

The effectiveness of nanovaccines mainly depends on the occurrence of immune responses mediated by CTLs. This reaction mainly includes three important factors: 1) spatiotemporal control of antigen delivery to LNs;[25,34,35] 2) cytoplasmic delivery and cross presentation of antigen in APCs;[36–38] 3) combined delivery of antigens and adjuvants.[11,12] The OVA@MMSNs@BM-Man nanovaccine meets the requirements of the above three factors. The prepared OVA@MMSNs@BM-Man nanovaccine can target DCs in LNs through the combination of mannose with CD205. In addition, the proper size of OVA@MMSNs@BM-Man nanovaccine also enables them to be directed towards LNs drainage. At the same time, the acidic degradation of MMSNs can promote the cross-presentation of antigen. Furthermore, the combined delivery of antigen (OVA) and immune adjuvants (BM and Mn^{2+}) can enhance the immunotherapeutic effects.

In summary, tumor nanovaccines as emerging technologies have significantly improved the feasibility of tumor vaccines. The mechanism and action sites of tumor nanovaccine were different from immune checkpoint inhibitors and immune cells. However, the efficacy of tumor nanovaccine is still influenced by the tumor microenvironment and inherent immune escape mechanisms, and often needs to be combined with other immune therapies (such as immune checkpoint inhibitors) to improve efficacy.

Conclusion

In this paper, OVA@MMSNs@BM-Man nanovaccine was constructed for targeted DCs-mediated immunotherapy. The nanovaccine displayed good targeting sability to DCs, and the generated Mn^{2+} can be used for MR imaging and activating cGAS-STING pathway. In combination with BM adjuvant, it can activate DCs for antigen presentation. The in vivo immune effects were verified in subcutaneous B16-OVA tumor model, and the results indicated that OVA@MMSNs@BM-Man nanovaccine could target LNs, activate DCs and further induce the generation of CTLs to exert anti-tumor effects. Compared with non-targeting group, OVA@MMSNs@BM-Man nanovaccine presented the highest tumor growth inhibition rate and extend the survival period of mice. We hope this paper will provide a new idea for tumor nanovaccines.

Data Sharing Statement

The data supporting this study's results are available from the corresponding author upon reasonable request.

Acknowledgments

Acknowledgments to the reviewers and editors for their valuable insights.

Author Contributions

All authors made a significant contribution to the work reported, whether that is in the conception, study design, execution, acquisition of data, analysis and interpretation, or in all these areas; took part in drafting, revising or critically reviewing the article; gave final approval of the version to be published; have agreed on the journal to which the article has been submitted; and agree to be accountable for all aspects of the work.

Funding

This work was sponsored by the National Natural Science Foundation of China (82302366), the Youth Fund Project of Natural Science Foundation of Jiangsu Province (BK20220663), the Startup Fund for Youth Talent in Xuzhou Medical University (D2021029), and the Integrated Innovation Project in Xuzhou Medical University (XYRHCX2021016).

Disclosure

The authors report no conflicts of interest in this work.

References

1. Sahin U, Tureci O. Personalized vaccines for cancer immunotherapy. Review. *Science*. 2018;359(6382):1355–1360. doi:10.1126/science.aar7112
2. Liu M, Feng Y, Lu Y, et al. Lymph-targeted high-density lipoprotein-mimetic nanovaccine for multi-antigenic personalized cancer immunotherapy. *Sci Adv*. 2024;10(11):eadk2444–eadk2444. doi:10.1126/sciadv.adk2444
3. Ji X, Yang H, Liu W, et al. Multifunctional parachute-like nanomotors for enhanced skin penetration and synergistic antifungal therapy. Article. *Acs Nano*. 2021;15(9):14218–14228. doi:10.1021/acsnano.1c01379
4. Liu G, Zhu M, Zhao X, Nie G. Nanotechnology-empowered vaccine delivery for enhancing CD8⁺ T cells-mediated cellular immunity. Review. *Adv. Drug Delivery Rev.* 2021;176113889. doi:10.1016/j.addr.2021.113889
5. Ni Q, Zhang F, Liu Y, et al. A bi-adjuvant nanovaccine that potentiates immunogenicity of neoantigen for combination immunotherapy of colorectal cancer. Article. *Sci Adv*. 2020;6(12):eaaw6071. doi:10.1126/sciadv.aaw6071
6. Pan C, Wu J, Qing S, et al. Biosynthesis of self-assembled proteinaceous nanoparticles for vaccination. Article. *Adv Materials*. 2020;32 (42):2002940. doi:10.1002/adma.202002940
7. Boyoglu-Barnum S, Ellis D, Gillespie RA, et al. Quadrivalent influenza nanoparticle vaccines induce broad protection. Article. *Nature*. 2021;592 (7855):623–+. doi:10.1038/s41586-021-03365-x
8. Luo M, Wang H, Wang Z, et al. A STING-activating nanovaccine for cancer immunotherapy. Article. *Nature Nanotechnol*. 2017;12(7):648–+. doi:10.1038/nnano.2017.52
9. Gong N, Zhang Y, Teng X, et al. Proton-driven transformable nanovaccine for cancer immunotherapy. Article. *Nature Nanotechnol*. 2020;15 (12):1053–U111. doi:10.1038/s41565-020-00782-3
10. Liu S, Jiang Q, Zhao X, et al. A DNA nanodevice-based vaccine for cancer immunotherapy. Article. *Nature Materials*. 2021;20(3):421–+. doi:10.1038/s41563-020-0793-6
11. Li AW, Sobral MC, Badrinath S, et al. A facile approach to enhance antigen response for personalized cancer vaccination. Article. *Nature Materials*. 2018;17(6):528–+. doi:10.1038/s41563-018-0028-2
12. Kuai R, Ochyl LJ, Bahjat KS, Schwendeman A, Moon JJ. Designer vaccine nanodiscs for personalized cancer immunotherapy. Article. *Nature Materials*. 2017;16(4):489–+. doi:10.1038/nmat4822
13. Liang J-L, Jin X-K, Zhang S-M, et al. Specific activation of cGAS-STING pathway by nanotherapeutics- mediated ferroptosis evoked endogenous signaling for boosting systemic tumor immunotherapy. Article. *Sci Bulletin*. 2023;68(6):622–636. doi:10.1016/j.scib.2023.02.027
14. Deng R, Xie X, Vendrell M, Chang Y-T, Liu X. Intracellular glutathione detection using MnO_2-nanosheet-modified upconversion nanoparticles. Article. *J Am Chemical Soc*. 2011;133(50):20168–20171. doi:10.1021/ja2100774
15. Yu L, Chen Y, Lin H, Gao S, Chen H, Shi J. Magnesium-engineered silica framework for pH-accelerated biodegradation and DNAzyme-triggered chemotherapy. Article. *Small*. 2018;14(35):1800708. doi:10.1002/smll.201800708
16. Zhao H, Wang J, Li X, et al. A biocompatible theranostic agent based on stable bismuth nanoparticles for X-ray computed tomography/magnetic resonance imaging-guided enhanced chemo/photothermal/chemodynamic therapy for tumours. Article. *J Colloid Interface Sci*. 2021;604:80–90. doi:10.1016/j.jcis.2021.06.174
17. Wang C, Guan Y, Lv M, et al. Manganese increases the sensitivity of the cGAS-STING pathway for double-stranded DNA and is required for the host defense against DNA viruses. Article. *Immunity*. 2018;48(4):675–+. doi:10.1016/j.immuni.2018.03.017
18. Hou L, Tian C, Yan Y, Zhang L, Zhang H, Zhang Z. Manganese-based nanoactivator optimizes cancer immunotherapy *via* enhancing innate immunity. Article. *Acs Nano*. 2020;14(4):3927–3940. doi:10.1021/acsnano.9b06111
19. Shakya M, Colin-Jones R, Theiss-Nyland K, et al. Phase 3 efficacy analysis of a typhoid conjugate vaccine trial in Nepal. Article. *N Engl J Med*. 2019;381(23):2209–2218. doi:10.1056/NEJMoa1905047
20. Pastural E, McNeil SA, MacKinnon-Cameron D, et al. Safety and immunogenicity of a 30-valent M protein-based group a streptococcal vaccine in healthy adult volunteers: a randomized, controlled Phase I study. Article. *Vaccine*. 2020;38(6):1384–1392. doi:10.1016/j.vaccine.2019.12.005
21. Thaiss CA, Zmora N, Levy M, Elinav E. The microbiome and innate immunity. Review. *Nature*. 2016;535:7610):65–74. doi:10.1038/nature18847
22. Kim OY, Park HT, Dinh NTH, et al. Bacterial outer membrane vesicles suppress tumor by interferon-γ- mediated antitumor response. Article. *Nature Communications*. 2017:8626. doi:10.1038/s41467-017-00729-8.
23. Silhavy TJ, Kahne D, Walker S. The bacterial cell envelope. Article. *Cold Spring Harbor Perspectives in Biol*. 2010;2(5):a000414. doi:10.1101/cshperspect.a000414
24. Chen L, Qin H, Zhao R, et al. Bacterial cytoplasmic membranes synergistically enhance the antitumor activity of autologous cancer vaccines. Article. *Sci Translational Med*. 2021;13(601):eabc2816. doi:10.1126/scitranslmed.abc2816
25. Conniot J, Scomparin A, Peres C, et al. Immunization with mannosylated nanovaccines and inhibition of the immune-suppressing microenvironment sensitizes melanoma to immune checkpoint modulators. Article. *Nature Nanotechnol*. 2019;14(9):891–+. doi:10.1038/s41565-019-0512-0
26. Li X, Zhang X, Zhao Y, Sun L. Fabrication of biodegradable Mn-doped mesoporous silica nanoparticles for pH/redox dual response drug delivery. Article. *J Inorganic Biochem*. 2020;202110887. doi:10.1016/j.jinorgbio.2019.110887
27. Wu X, Wen X, Lin X, et al. pH/glutathione-responsive theranostic nanoprobes for chemoimmunotherapy and magnetic resonance imaging of ovarian cancer cells. Article. *Colloids Surf B Biointerfaces*. 2024:241114053. doi:10.1016/j.colsurfb.2024.114053.
28. Chong L, Jiang Y-W, Wang D, Chang P, Xu K, Li J. Targeting and repolarizing M2-like tumor-associated macrophage-mediated MR imaging and tumor immunotherapy by biomimetic nanoparticles. Article. *J Nanobiotechnol*. 2023;21(1):401. doi:10.1186/s12951-023-02122-8
29. Gao F, Tang Y, Liu W-L, et al. Intra/extracellular lactic acid exhaustion for synergistic metabolic therapy and immunotherapy of tumors. Article. *Adv Materials*. 2019;31(51):1904639. doi:10.1002/adma.201904639
30. Gao Z-L, Xu W, Zheng S-J, Duan Q-J, Liu R, Du J-Z. Orchestrated cytosolic delivery of antigen and adjuvant by manganese ion-coordinated nanovaccine for enhanced cancer immunotherapy. *Nano Lett*. 2023;23(5):1904–1913. doi:10.1021/acs.nanolett.2c04970

31. Jang D-I, Lee AH, Shin H-Y, et al. The Role of Tumor Necrosis Factor Alpha (TNF-α) in autoimmune disease and current TNF-α Inhibitors in Therapeutics. Review. *Int J mol Sci*. 2021;22(5):2719. doi:10.3390/ijms22052719
32. Jorgovanovic D, Song M, Wang L, Zhang Y. Roles of IFN-γ in tumor progression and regression: a review. *Review Biomarker Res*. 2020;8(1):49. doi:10.1186/s40364-020-00228-x
33. Saxena M, van der Burg SH, Melief CJM, Bhardwaj N. Therapeutic cancer vaccines. Review. *Nat Rev Cancer*. 2021;21(6):360–378. doi:10.1038/s41568-021-00346-0
34. Reddy ST, Rehor A, Schmoekel HG, Hubbell JA, Swartz MA. In vivo targeting of dendritic cells in lymph nodes with poly(propylene sulfide) nanoparticles. Article. *J Controlled Rel*. 2006;112(1):26–34. doi:10.1016/j.jconrel.2006.01.006
35. Jin H, Qian Y, Dai Y, et al. Magnetic enrichment of dendritic cell vaccine in lymph node with fluorescent-magnetic nanoparticles enhanced cancer immunotherapy. Article. *Theranostics*. 2016;6(11):2000–2014. doi:10.7150/thno.15102
36. Xu J, Lv J, Zhuang Q, et al. A general strategy towards personalized nanovaccines based on fluoropolymers for post-surgical cancer immunotherapy. Article. *Nature Nanotechnol*. 2020;15(12):1043–U92. doi:10.1038/s41565-020-00781-4
37. Zhang X-Q, Xu X, Bertrand N, Pridgen E, Swami A, Farokhzad OC. Interactions of nanomaterials and biological systems: implications to personalized nanomedicine. Review. *Adv Drug Deliv Rev*. 2012;64(13):1363–1384. doi:10.1016/j.addr.2012.08.005
38. Yu X, Dai Y, Zhao Y, et al. Melittin-lipid nanoparticles target to lymph nodes and elicit a systemic anti-tumor immune response. Article. *Nature Communications*. 2020;11(1):1110. doi:10.1038/s41467-020-14906-9